Editors' Suggestion

Momentum-resolved observation of ultrafast interlayer charge transfer between the topmost layers of MoS_2

R. Wallauer,[1,*] P. Marauhn,[2] J. Reimann,[1] S. Zoerb,[3] F. Kraus,[3] J. Güdde,[1] M. Rohlfing,[2] and U. Höfer[1]

[1]*Fachbereich Physik und Zentrum für Materialwissenschaften, Philipps-Universität, 35032 Marburg, Germany*

[2]*Institut für Festkörpertheorie, Westfälische Wilhelms-Universität Münster, 48149 Münster, Germany*

[3]*Fachbereich Chemie, Philipps-Universität, 35032 Marburg, Germany*

(Received 20 March 2020; revised 17 August 2020; accepted 20 August 2020; published 11 September 2020)

We report on the direct observation of electron transfer between the surface and the second layer of the prototypical transition-metal dichalcogenide 2H-MoS_2. We are able to disentangle the excitation and the transfer process in our measurement. Thereby, we determine both the momentum location and the duration of the electron transfer between the first two layers. Our *GW*-based tight-binding calculations reveal that the band gap in the surface layer is considerably larger than in deeper layers and that the coupling between surface and deeper layers is strongly momentum-dependent throughout the Brillouin zone. At the conduction-band minimum $\bar{\Sigma}$ we find strong coupling, which explains the ultrafast interlayer charge transfer observed in our experiment at this location.

DOI: 10.1103/PhysRevB.102.125417

I. INTRODUCTION

Heterostructures built from monolayer sheets of two-dimensional materials exhibit a variety of physical phenomena, such as unusual superconductivity [1], topological ordered phases [2], or moire excitons [3,4]. Many possible applications based on optoelectronic devices have been proposed, in particular for transition-metal dichalcogenide semiconductors (TMDs) [5–7]. However, a microscopic understanding of the charge transfer between layers of these materials has not yet been well developed, although it is of crucial interest for the design of such devices [8].

In semiconducting TMDs, the interlayer charge transfer after optical excitation is usually related to the formation of an interlayer exciton, which can be observed by means of optical experiments. The separation of electrons and holes proceeds on an ultrafast timescale and leads to a broadening of the resonance linewidth, quenching of photoluminescence, or transient reflectivity changes, which are the most common optical probes to study such ultrafast transfer. The transfer times of electrons and holes determined in this way show a wide spread, with reported values ranging from 40–50 fs [9–11] up to 500 fs [12–14].

The nature of the interlayer charge transfer is still controversial [8] for mainly two reasons. First, most of the observed transfer times are found to be robust against momentum mismatch of the heterostructure constituents [9,15]. Only recently have significantly longer interlayer exciton formation times been reported, which depend strongly on the stacking angle [14]. Secondly, fast interlayer transfer times should be related to strong interlayer coupling. However, the charge transfer in heterostructure samples presumably takes place at the $\bar{K}$-valleys of either material where the interlayer coupling is weak. Therefore, some theoretical models suggest a coherent nature of the transfer process [16] or the involvement of momentum locations where the coupling between layers is stronger, namely at the conduction-band minimum $\bar{\Sigma}$ [17,18]. Other theoretical studies predict transfer processes mediated by phonon excitation [19,20] or hot electrons [21].

In this work, we show that the electron transfer between the topmost layers of a 2H-MoS_2-crystal, which means in the case of ideal stacking (i.e., 180°), is located at $\bar{\Sigma}$ and proceeds on a timescale of less than 20 fs. We employ time- and angle-resolved two-photon photoemission (2PPE) spectroscopy with a high-harmonic probe (HHG-2PPE), which allows us to image the population dynamics of initially unoccupied electronic states and the charge transfer directly in momentum space [22–26]. The experimental findings are complemented by theoretical calculations using a tight-binding model combined with the *GW* method in the LDA+*GdW* approximation [27,28].

II. EXPERIMENT

Figure 1 illustrates the design of the experiment together with a scheme of the observed charge-transfer processes. We have recently shown that the electronic excitation after photon absorption above the first-layer band gap in bulk 2H-MoS_2 resides at $\bar{K}$, as in the monolayer systems [24]. Our theoretical calculations show that, at $\bar{K}$, the surface layer decouples from the bulk. Further experimental evidence for the decoupling of the surface layer from the bulk is provided by the observation of valley selectivity in spin-resolved detection [23] or excitation [25]. Strikingly, our results show that the surface layer has its own band gap, which is significantly larger than in deeper layers. This is illustrated in Fig. 1 by different colors of the

*Corresponding author: robert.wallauer@physik.uni-marburg.de

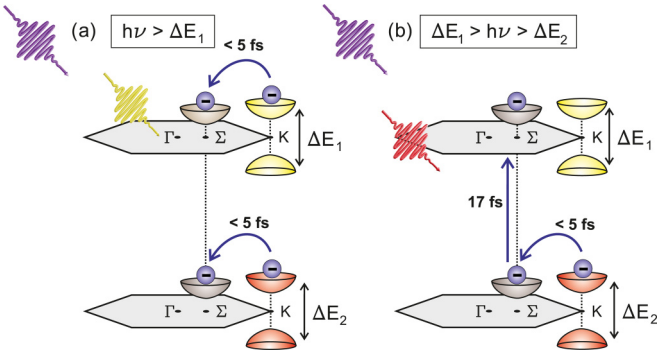

FIG. 1. Scheme of the experiment. Electrons are excited by tunable visible pump pulses and probed by XUV photons. Emitted electrons are detected in a hemispherical electron analyzer along $\bar{\Sigma}$-$\bar{K}$. Only electrons from the surface layer contribute to the 2PPE signal. The layer-dependent size of the band gap, indicated by different colors of the K valleys, allows us to excite the system within different layers by tuning the pump-pulse photon energy, and to study electron transfer between layers. (a) Excitation above or close to the surface layer gap. Electrons within each layer are excited at $\bar{K}$ and transferred to $\bar{\Sigma}$ within 5 fs. (b) Excitation between surface and second layer gap. Only electrons in deeper layers are excited at $\bar{K}$, and the transfer between layers at this momentum location is suppressed due to the larger gap and weak coupling. After the fast transfer to $\bar{\Sigma}$ within deeper layers, electrons are transferred to the surface layer due to the strong coupling at $\bar{\Sigma}$.

K-valleys. Therefore, we can excite electrons either within the surface layer [Fig. 1(a)] or within lower-lying layers [Fig. 1(b)] by tuning the photon energy of pump pulses above or below the surface layer gap, respectively. Electrons are subsequently photoemitted by an XUV probe pulse and detected in a hemispherical electron analyzer along the $\bar{\Sigma}$-$\bar{K}$ direction. With our technique, we selectively probe the surface layer, since the escape depth of 20-eV photoelectrons detected here is particular small (∼5 Å), a fact that has been exploited in previous time-resolved and static photoemission experiments from TMD samples before [23,25,26,29–31]. The sensitivity to probe the population within only the surface layer together with the selectivity of the pump pulse allows us to distinguish between interlayer and intralayer charge transfer.

For a detailed description of our experimental setup, we refer to [24,32]. The HHG source is operated at 100 kHz, and we use the 15th harmonic of the fundamental 800-nm laser pulses, resulting in a probe photon energy of 23.25 eV. Tunable pump pulses with photon energies between 600 and 685 nm (1.81–2.07 eV) are generated in an optical parametric amplifier. Pulse length is around 50 fs, and we apply pump fluences of approximately 100 μJ/cm^2 on the sample.

III. RESULTS AND DISCUSSION

A. Excitation dynamics

Figures 2(a) and 2(b) show the energy-momentum maps for different time delays between pump and probe pulse around temporal overlap for two excitation energies. In the case of excitation above the surface layer gap ($h\nu = 2.07$ eV), a 2PPE signal localized at $\bar{K}$ appears at temporal overlap and is visible over the complete observed time range. We assign this long living signal to an occupation of the local conduction-band minimum at $\bar{K}$. At a pump photon energy of 1.81 eV, we do not observe an occupation of the conduction

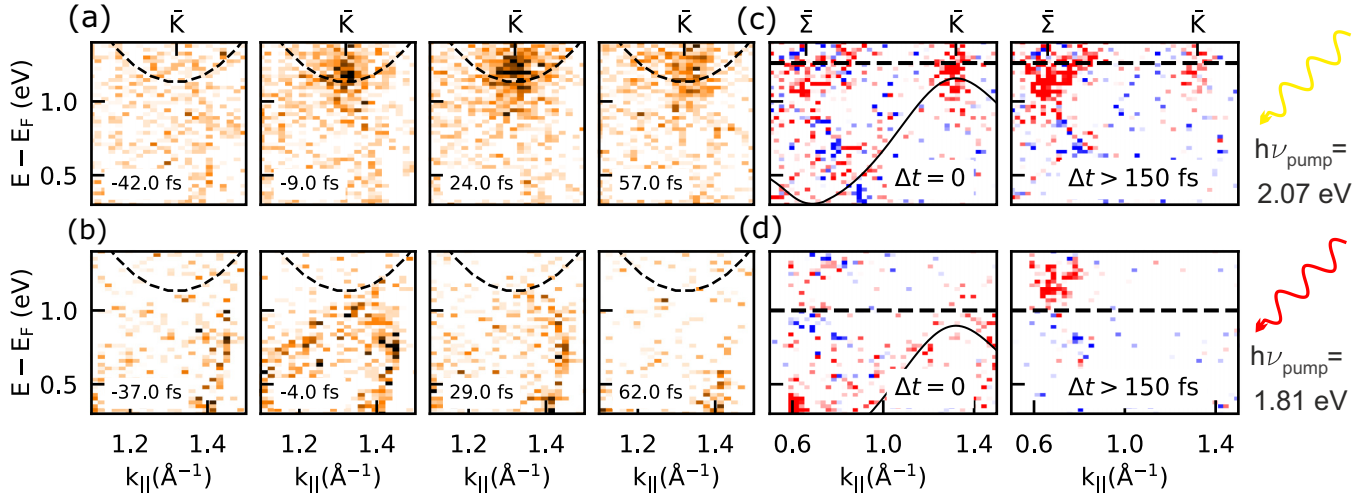

FIG. 2. Dynamics and energetic positions of excited electrons in the surface layer. Energy-momentum maps of the initial stages of electron excitation around $\bar{K}$ for a pump photon energy (a) above the surface layer band gap and (b) below the surface layer gap for different pump-probe delays Δt. In the case of above surface layer band-gap excitation, an electron population localized at $\bar{K}$ is clearly visible around temporal overlap, which significantly decreases for larger delays but never vanishes in our observed time interval. In contrast, for pump photon energies below the surface layer band gap, only a faint replica of the valence band is observed around temporal overlap, which we attribute to nonresonant photoemission. (c),(d) Comparison of the 2PPE signal within the complete momentum range of the experiment for the temporal overlap and for long delays. A population at both high symmetry points is clearly visible already around temporal overlap in the case of high excitation energies (c), whereas only the conduction-band minimum at $\bar{\Sigma}$ is populated for low excitation energies (d). Dashed lines indicate the excitation threshold for the surface layer (valence-band maximum + pump photon energy).

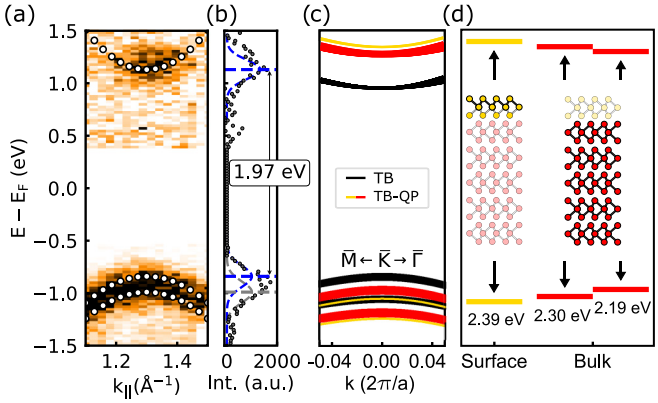

FIG. 3. (a) Energy-momentum map of the valence band and populated conduction band. The unoccupied part is integrated over delays $\Delta t > 150$ fs, where we observe no significant change in the population. (b) The energy distribution curve is a projection ± 0.03 Å around $\bar{K}$. From fits to the EDC we extract a surface layer band gap at $\bar{K}$ of 1.97 eV. (c) Band structure (around $\bar{K}$) calculated for a slab of 40-layer MoS_2 using conventional TB and our TB-QP approach. (d) Schematic energy level diagram of the calculated bands (TB-QP) at $\bar{K}$. The surface layer is largely decoupled from the other layers of the slab and has the largest band gap (2.39 eV). The band gaps of the other layers, which are summarized as bulk, are smaller and range from 2.30 to 2.19 eV. The extracted band gaps illustrate that the surface layer is decoupled from lower-lying layers.

band at $\bar{K}$. In this case, the excitation is too far below the resonance for the surface layer, and the only visible signal at this momentum location stems from the nonresonant 2PPE process, which is the simultaneous absorption of a pump and probe photon. Its signature is a replica of the valence band within a time window given by the cross-correlation of the two laser pulses. It is faintly visible in the two images closest to temporal overlap.

In Figs. 2(c) and 2(d) we compare energy-momentum maps over a larger momentum range at two stages of their temporal evolution to highlight the differences between the two excitation schemes. These maps include both high symmetry points, $\bar{K}$ and $\bar{\Sigma}$, around temporal overlap (left) and at long delays (right). We subtracted a constant background, which has been recorded at negative delays, where no pump pulse is present, from these images. A thin solid line indicates the position of the nonresonant contribution around temporal overlap. The highest excitation energy, given by the energetic position of the valence-band maximum at $\bar{K}$ and the pump photon energy, is indicated by the thick dashed line for the respective case. For the low pump photon energy, the absence of any population around $\bar{K}$ is evident, despite the appearance of a signal at $\bar{\Sigma}$ at longer delays. In the case of the higher pump photon energies, charge redistribution from $\bar{K}$ to $\bar{\Sigma}$ is clearly visible when comparing the two different time steps.

For excitation with photon energies higher than 1.89 eV, the population of a long living state in the conduction band at $\bar{K}$ is clearly visible [see Fig. 3(a)]. To determine the band gap at $\bar{K}$, we evaluate the energetic position of the spin-split valence band by fitting a superposition of two Gaussian line profiles to the energy distribution curve [EDC, Fig. 3(b)]. In the unoccupied part of the spectrum, the shape of the line profile is slightly asymmetric, indicating a nonequilibrated electron distribution. We extract a band gap of 1.97 eV from the upper valence band to the low-energy side of the conduction-band energy curve. We obtain the same gap value when we excite the system with pump photon energies up to 2.07 eV, which indicates that we are observing the unperturbed energetic position of this intermediate state in the 2PPE process. This is consistent with the fact that we are in the weak excitation regime, and our spectra show no sign of band renormalization as observed in other experiments at higher excitation densities [29].

B. Band structure calculations

To understand the energy dependence of the population dynamics presented in Fig. 2, we perform theoretical calculations on the electronic structure of bulklike MoS_2. The surface of the bulk crystal is taken into account by employing a slab geometry of sufficient thickness. We use a tight-binding (TB) model to reproduce the band structure obtained within density functional theory (DFT), and we extend it to include polarization effects by means of layer-resolved *GW* quasiparticle corrections (TB-QP). Details on the model are provided in the Supplemental Material [33]. Figure 3(c) shows the band structure in the vicinity of the $\bar{K}$-point calculated for a slab of 40 layers MoS_2 using conventional TB and our TB-QP approach. As a result of the underlying *GW* calculation, our TB-QP approach exhibits a larger gap than the DFT-based conventional TB [34]. More importantly, some bands emerge from the original branches as they shift more than others. Analyzing the corresponding wave functions, these bands stem predominantly (>85%) from the surface layer of the slab. It is the difference in the dielectric environment that shifts the bands of the surface layer such that interaction and, hence, hybridization with bands of the other layers are largely suppressed. As a result, the surface layer decouples from the other layers and has its own band gap (2.39 eV) that is significantly larger than in deeper layers [2.30–2.19 eV; see Fig. 3(d)]. It should be noted that our TB-QP energies are larger than our experimental data for several reasons. Our experiments are performed at room temperature, thus showing a gap closing of about 0.1 eV due to electron-phonon interactions. Moreover, our LDA+*GdW* version of the *GW* method tends to overestimate the band gap of MoS_2. Note that neither of these effects concerns the observed energetic decoupling of the surface layer from the other layers. Our theoretical results suggest that excitation at higher energy predominantly populates the surface layer at $\bar{K}$, while lower excitation energy populates deeper layers (but still at $\bar{K}$) instead. Furthermore, we conclude that electron transfer to the surface layer at $\bar{K}$ is strongly suppressed due to weak coupling between surface and deeper layers and the mismatch in gap size.

C. Interlayer coupling and transfer dynamics

In Fig. 4 we show a quantitative analysis of the 2PPE intensities together with the conduction-band coupling between the surface layer and all other layers of the bulklike slab. The time evolution of the electron intensities at $\bar{K}$ is shown in Fig. 4(a). We describe the time evolution of the electron intensities for all pump photon energies with a dynamical simulation,

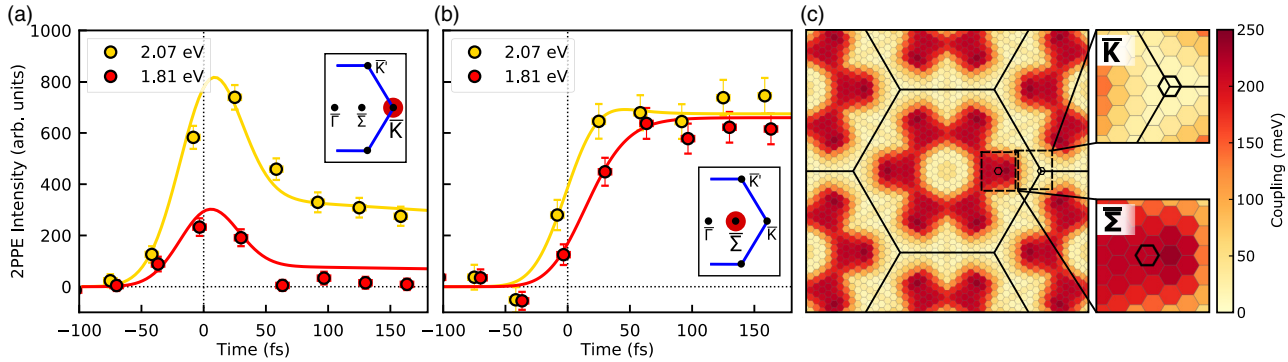

FIG. 4. (a) Time evolution of the 2PPE signal at $\bar{K}$ for excitation energies above (yellow) and below (red) the surface layer gap. Solid lines are fits from a dynamical model of 2PPE intensities. (b) Time evolution of the 2PPE signal at $\bar{\Sigma}$ for the same excitation energies as in (a). A rate equation model (solid lines) resulting in an electron transfer time between layers of 17 fs gives remarkable agreement with the experimental data points. (c) Conduction-band coupling between the surface layer and all other layers of bulklike MoS_2 (slab of 40 layers). The coupling is calculated within our TB-QP approach on a $24 \times 24 \times 1$ k-space grid between all subbands of the two lowest conduction bands.

which has been described in detail before [35]. In short, we are solving the optical Bloch equations for a three level-system numerically. We take into account one well-defined intermediate state and a free-electron final state. Detuning of the pump pulse with respect to the intermediate state and its temporal width is taken from the measurement. Only fit parameters are the dephasing time of the intermediate state and its finite lifetime. Our model is in very good agreement with the measurement assuming a dephasing time of 200 fs and a lifetime of around 1 ps for the conduction band at $\bar{K}$. Within this model, the fast rise and decay of the time evolution can be clearly assigned to the nonresonant contribution to the electron signal, while the dynamics after 100 fs can be solely assigned to a population of the intermediate state.

Figure 4(b) shows the population dynamics at the $\bar{\Sigma}$-point for both of the aforementioned excitation energies. Neither curve resembles the fast dynamics of the temporal overlap region at $\bar{K}$, indicating the absence of a direct excitation at this high symmetry point. However, the conduction-band minimum at $\bar{\Sigma}$ is populated extremely fast after excitation. Within our rate equation model (solid lines) we find good agreement for transfer times from $\bar{K}$ to $\bar{\Sigma}$ well below 5 fs. In the case of excitation with the large detuning, we observe a significantly delayed occupation. This coincides with the absence of a visible population at $\bar{K}$.

Consistent with this picture, we simulate in a few-layer rate equation model the convergence of the population in the first layers of a bulk. In this simulation, we assume an excitation within each layer, depending on detuning relative to the gap at $\bar{K}$. We further assume the same ultrafast intralayer $\bar{K}$-$\bar{\Sigma}$ transfer time for each layer, since we have observed this transfer time to be largely independent for all small detunings. At $\bar{\Sigma}$, strong coupling between all layers, including the surface layer, leads to a convergence of the populations among the total system on an ultrafast timescale, followed by a diffusion into the bulk on a much larger timescale. In the case of high pump photon energies, the almost equal population of excited electrons in each layer leads to almost no interlayer transfer. The significant delay in the time evolution in the case of low pump photon energy is in very good agreement with an interlayer transfer time of 17 ± 5 fs.

This process is supported by the momentum-dependent conduction-band coupling between the surface layer and all other layers, as shown in Fig. 4(c). The coupling, evaluated within our TB-QP approach, represents an effective coupling matrix element between the surface and all other layers, taking all subbands of the lowest two conduction bands into account. Details on the calculation are given in the Supplemental Material [33]. The coupling between surface and bulk varies across the entire Brillouin zone. Most importantly, the situation at $\bar{\Sigma}$ differs significantly from that at $\bar{K}$. While at $\bar{K}$ the coupling is vanishingly small, in line with the results above, the $\bar{\Sigma}$-point is situated in a region of strong coupling between surface and bulk.

IV. CONCLUSION

The electron transfer studied in this work is to our knowledge the fastest interlayer charge transfer in TMDs observed so far. In this context, transfer times reported here have to be considered as a lower limit, given the momentum match of layers in a single-crystal and the transfer being located at a point of strong interlayer coupling. In addition, our experimental technique allows us to separate the charge transfer at $\bar{\Sigma}$ from all other processes that contribute to signals in all-optical methods. Hence, we obtain here the bare interlayer transfer time.

Our findings are in very good agreement with theoretical predictions [17,18], which describe charge transfer in TMD heterostructures via $\bar{\Sigma}$ instead of $\bar{K}$-$\bar{K}$. While in our case the electron transfer at $\bar{K}$ is energetically unfavorable and therefore cannot be excluded for other band alignments, we were able to show a significant decoupling at this momentum location driven by environmental screening. In contrast, coupling between surface and deeper layers at $\bar{\Sigma}$ is strong, which explains the ultrafast charge transfer times observed in experiment.

ACKNOWLEDGMENTS

Funding was provided by the Deutsche Forschungsgemeinschaft (DFG, German Research Foundation), Project-ID 223848855-SFB 1083.

[1] Y. Cao, V. Fatemi, S. Fang, K. Watanabe, T. Taniguchi, E. Kaxiras, and P. Jarillo-Herrero, Unconventional superconductivity in magic-angle graphene superlattices, Nature (London) **556**, 43 (2018).

[2] E. M. Spanton, A. A. Zibrov, H. Zhou, T. Taniguchi, K. Watanabe, M. P. Zaletel, and A. F. Young, Observation of fractional Chern insulators in a van der Waals heterostructure, Science **360**, 62 (2018).

[3] K. Tran, G. Moody, F. Wu, X. Lu, J. Choi, K. Kim, A. Rai, D. A. Sanchez, J. Quan, A. Singh, J. Embley, A. Zepeda, M. Campbell, T. Autry, T. Taniguchi, K. Watanabe, N. Lu, S. K. Banerjee, K. L. Silverman, S. Kim, E. Tutuc, L. Yang, A. H. MacDonald, and X. Li, Evidence for moiré excitons in van der Waals heterostructures, Nature (London) **567**, 71 (2019).

[4] C. Jin, E. C. Regan, A. Yan, M. Iqbal Bakti Utama, D. Wang, S. Zhao, Y. Qin, S. Yang, Z. Zheng, S. Shi, K. Watanabe, T. Taniguchi, S. Tongay, A. Zettl, and F. Wang, Observation of moiré excitons in WSe_2/WS_2 heterostructure superlattices, Nature (London) **567**, 76 (2019).

[5] B. Radisavljevic, A. Radenovic, J. Brivio, V. Giacometti, and A. Kis, Single-layer MoS_2 transistors, Nat. Nanotechnol. **6**, 147 (2011).

[6] A. Pospischil, M. M. Furchi, and T. Mueller, Solar-energy conversion and light emission in an atomic monolayer P-N diode, Nat. Nanotechnol. **9**, 257 (2014).

[7] W. Z. Wu, L. Wang, Y. L. Li, F. Zhang, L. Lin, S. M. Niu, D. Chenet, X. Zhang, Y. F. Hao, T. F. Heinz, J. Hone, and Z. L. Wang, Piezoelectricity of single-atomic-layer MoS_2 for energy conversion and piezotronics, Nature (London) **514**, 470 (2014).

[8] C. H. Jin, E. Y. Ma, O. Karni, E. C. Regan, F. Wang, and T. F. Heinz, Ultrafast dynamics in van der Waals heterostructures, Nat. Nanotechnol. **13**, 994 (2018).

[9] H. M. Zhu, J. Wang, Z. Z. Gong, Y. D. Kim, J. Hone, and X. Y. Zhu, Interfacial charge transfer circumventing momentum mismatch at two-dimensional van der Waals heterojunctions, Nano Lett. **17**, 3591 (2017).

[10] X. P. Hong, J. Kim, S. F. Shi, Y. Zhang, C. H. Jin, Y. H. Sun, S. Tongay, J. Q. Wu, Y. F. Zhang, and F. Wang, Ultrafast charge transfer in atomically thin MoS_2/WS_2 heterostructures, Nat. Nanotechnol. **9**, 682 (2014).

[11] H. L. Chen, X. W. Wen, J. Zhang, T. M. Wu, Y. J. Gong, X. Zhang, J. T. Yuan, C. Y. Yi, J. Lou, P. M. Ajayan, W. Zhuang, G. Y. Zhang, and J. R. Zheng, Ultrafast formation of interlayer hot excitons in atomically thin MoS_2/WS_2 heterostructures, Nat. Commun. **7**, 12512 (2016).

[12] F. Ceballos, M. Z. Bellus, H. Y. Chiu, and H. Zhao, Ultrafast charge separation and indirect exciton formation in a MoS_2-$MoSe_2$ van der Waals heterostructure, ACS Nano **8**, 12717 (2014).

[13] Z. H. Ji, H. Hong, J. Zhang, Q. Zhang, W. Huang, T. Cao, R. X. Qiao, C. Liu, J. Liang, C. H. Jin, L. Y. Jiao, K. B. Shi, S. Meng, and K. H. Liu, Robust stacking-independent ultrafast charge transfer in MoS_2/WS_2 bilayers, ACS Nano **11**, 12020 (2017).

[14] P. Merkl, F. Mooshammer, P. Steinleitner, A. Girnghuber, K. Q. Lin, P. Nagler, J. Holler, C. Schüller, J. M. Lupton, T. Korn, S. Ovesen, S. Brem, E. Malic, and R. Huber, Ultrafast transition between exciton phases in van der Waals heterostructures, Nat. Mater. **18**, 691 (2019).

[15] H. Heo, J. H. Sung, S. Cha, B. G. Jang, J. Y. Kim, G. Jin, D. Lee, J. H. Ahn, M. J. Lee, J. H. Shim, H. Choi, and M. H. Jo, Interlayer orientation-dependent light absorption and emission in monolayer semiconductor stacks, Nat. Commun. **6**, 7372 (2015).

[16] F. Ceballos, M. G. Ju, S. D. Lane, X. C. Zeng, and H. Zhao, Highly efficient and anomalous charge transfer in van der Waals trilayer semiconductors, Nano Lett. **17**, 1623 (2017).

[17] Y. Wang, Z. Wang, W. Yao, G. B. Liu, and H. Y. Yu, Interlayer coupling in commensurate and incommensurate bilayer structures of transition-metal dichalcogenides, Phys. Rev. B **95**, 115429 (2017).

[18] P. Zereshki, Y. Q. Wei, R. Long, and H. Zhao, Layer-coupled states facilitate ultrafast charge transfer in a transition metal dichalcogenide trilayer heterostructure, J. Phys. Chem. Lett. **9**, 5970 (2018).

[19] Q. J. Zheng, W. A. Saidi, Y. Xie, Z. G. Lan, O. V. Prezhdo, H. Petek, and J. Zhao, Phonon-assisted ultrafast charge transfer at van der Waals heterostructure interface, Nano Lett. **17**, 6435 (2017).

[20] Q. J. Zheng, Y. Xie, Z. G. Lan, O. V. Prezhdo, W. A. Saidi, and J. Zhao, Phonon-coupled ultrafast interlayer charge oscillation at van der Waals heterostructure interfaces, Phys. Rev. B **97**, 205417 (2018).

[21] J. Zhang, H. Hong, J. Zhang, H. X. Fu, P. W. You, J. Lischner, K. H. Liu, E. Kaxiras, and S. Meng, New pathway for hot electron relaxation in two-dimensional heterostructures, Nano Lett. **18**, 6057 (2018).

[22] T. Rohwer, S. Hellmann, M. Wiesenmayer, C. Sohrt, A. Stange, B. Slomski, A. Carr, Y. W. Liu, L. M. Avila, M. Kallane, S. Mathias, L. Kipp, K. Rossnagel, and M. Bauer, Collapse of long-range charge order tracked by time-resolved photoemission at high momenta, Nature (London) **471**, 490 (2011).

[23] J. M. Riley, F. Mazzola, M. Dendzik, M. Michiardi, T. Takayama, L. Bawden, C. Granerod, M. Leandersson, T. Balasubramanian, M. Hoesch, T. K. Kim, H. Takagi, W. Meevasana, P. Hofmann, M. S. Bahramy, J. W. Wells, and P. D. C. King, Direct observation of spin-polarized bulk bands in an inversion-symmetric semiconductor, Nat. Phys. **10**, 835 (2014).

[24] R. Wallauer, J. Reimann, N. Armbrust, J. Güdde, and U. Höfer, Intervalley scattering in MoS_2 imaged by two-photon photoemission with a high-harmonic probe, Appl. Phys. Lett. **109**, 162102 (2016).

[25] R. Bertoni, C. W. Nicholson, L. Waldecker, H. Hübener, C. Monney, U. De Giovannini, M. Puppin, M. Hoesch, E. Springate, R. T. Chapman, C. Cacho, M. Wolf, A. Rubio, and R. Ernstorfer, Generation and Evolution of Spin-, Valley- and Layer-Polarized Excited Carriers in Inversion-Symmetric WSe_2, Phys. Rev. Lett. **117**, 277201 (2016).

[26] H. Beyer, G. Rohde, A. Grubisic Cabo, A. Stange, T. Jacobsen, L. Bignardi, D. Lizzit, P. Lacovig, C. E. Sanders, S. Lizzit, K. Rossnagel, P. Hofmann, and M. Bauer, 80% Valley Polarization of Free Carriers in Singly Oriented Single-Layer WS_2 on Au(111), Phys. Rev. Lett. **123**, 236802 (2019).

[27] M. Rohlfing, Electronic excitations from a perturbative LDA + *GdW* approach, Phys. Rev. B **82**, 205127 (2010).

[28] M. Drüppel, T. Deilmann, J. Noky, P. Marauhn, P. Krüger, and M. Rohlfing, Electronic excitations in transition metal dichalcogenide monolayers from an LDA + *GdW* approach, Phys. Rev. B **98**, 155433 (2018).

[29] F. Liu, M. E. Ziffer, K. R. Hansen, J. Wang, and X. Y. Zhu, Direct Determination of Band-Gap Renormalization in the Photoexcited Monolayer MoS_2, Phys. Rev. Lett. **122**, 246803 (2019).

[30] P. Hein, A. Stange, K. Hanff, L. X. Yang, G. Rohde, K. Rossnagel, and M. Bauer, Momentum-resolved hot electron dynamics at the 2H-MoS_2 surface, Phys. Rev. B **94**, 205406 (2016).

[31] S. Ulstrup, A. G. Cabo, D. Biswas, J. M. Riley, M. Dendzik, C. E. Sanders, M. Bianchi, C. Cacho, D. Matselyukh, R. T. Chapman, E. Springate, P. D. C. King, J. A. Miwa, and P. Hofmann, Spin and valley control of free carriers in single-layer WS_2, Phys. Rev. B **95**, 041405(R) (2017).

[32] C. M. Heyl, J. Güdde, A. L'Huillier, and U. Höfer, High-order harmonic generation with μJ laser pulses at high repetition rates, J. Phys. B **45**, 074020 (2012).

[33] See Supplemental Material at http://link.aps.org/supplemental/10.1103/PhysRevB.102.125417 for details on band-structure calculations, which includes Refs. [34,36–42].

[34] F. Zahid, L. Liu, Y. Zhu, J. Wang, and H. Guo, A generic tight-binding model for monolayer, bilayer and bulk MoS_2, AIP Adv. **3**, 052111 (2013).

[35] T. Klamroth, P. Saalfrank, and U. Höfer, Open-system density-matrix approach to image-potential dynamics of electrons at Cu(100): Energy- and time-resolved two-photon photoemission spectra, Phys. Rev. B **64**, 035420 (2001).

[36] M. S. Hybertsen and S. G. Louie, Theory of quasiparticle surface states in semiconductor surfaces, Phys. Rev. B **38**, 4033 (1988).

[37] M. Rohlfing, P. Krüger, and J. Pollmann, Quasiparticle band-structure calculations for C, Si, Ge, GaAs, and SiC using Gaussian-orbital basis-sets, Phys. Rev. B **48**, 17791 (1993).

[38] G. Onida, L. Reining, and A. Rubio, Electronic excitations: density-functional versus many-body Green's-function approaches, Rev. Mod. Phys. **74**, 601 (2002).

[39] M. Rohlfing, Redshift of Excitons in Carbon Nanotubes Caused by the Environment Polarizability, Phys. Rev. Lett. **108**, 087402 (2012).

[40] A. Arora, T. Deilmann, P. Marauhn, M. Drüppel, R. Schneider, M. R. Molas, D. Vaclavkova, S. M. de Vasconcellos, M. Rohlfing, M. Potemski, and R. Bratschitsch, Valley-contrasting optics of interlayer excitons in Mo- and W-based bulk transition metal dichalcogenides, Nanoscale **10**, 15571 (2018).

[41] M. Drüppel, T. Deilmann, P. Krüger, and M. Rohlfing, Diversity of trion states and substrate effects in the optical properties of an MoS_2 monolayer, Nat. Commun. **8**, 2117 (2017).

[42] G. Krabbes, H. Oppermann, and J. Henke, Chemischer Transport und thermische Stabilität von Sulfidphasen des Molybdäns, Z. Anorg. Allg. Chem. **470**, 7 (1980).